Available online at www.sciencedirect.com
ScienceDirect
Journal of Sound and Vibration 300 (2007) 676–694
JOURNAL OF SOUND AND VIBRATION
www.elsevier.com/locate/jsvi

Damped lateral vibrations of straight and curved cables with no axial pre-load

Miha Otrin, Miha Boltežar*

University of Ljubljana, Faculty of Mechanical Engineering, Aškerčeva 6, 1000 Ljubljana, SI Slovenia

Received 1 November 2005; received in revised form 15 June 2006; accepted 14 August 2006
Available online 16 October 2006

Abstract

This paper presents a study of the lateral vibrations of straight and curved cables with no axial pre-load. For the computation of the vibration transmissibility we used finite elements based on the Euler–Bernoulli theory. The dissipation of energy was studied with viscous- and structural-damping models, where the Rayleigh coefficients and the frequency dependence of the loss factor were identified. By using the equality between the measured and the computed natural frequencies the frequency dependence of the dynamic modulus of elasticity was estimated and used for all the studied types of cable. The excitation was the result of moving the support in a direction perpendicular to the axis of the cable. The mathematical model for the computation of the vibrations of the straight and curved cables was verified with experimental measurements in which the support excitation was achieved with an electrodynamic shaker and the amplitude force was measured at the fixed support with a dynamometer. For the curved cable the mathematical model was verified for in-plane and out-off-plane vibrations. Three straight cables of different lengths were analyzed for the dependence of the Rayleigh coefficients on the length of the cables.

1. Introduction

Recently, the automotive industry has had a requirement for modeling the lateral vibrations of steel cables with no axial pre-load. A large number of investigations into the dynamic behavior of cables where the axial load on the cable was much greater than the bending load have been carried out. Many investigations of cable statics and dynamics were carried out by Costello [1]. He modeled a strand of cable with several thin wires, where the center wire is of sufficient size to prevent the outer wires from touching each other. Nawrocki and Labrosse [2] presented a finite-element model of a simple straight wire rope strand. His model has proved to be reliable in comparison with experimental data for every possible interwire motion. He considered either a pure axial load or an axial load combined with a bending load. Koh and Rong [3] modeled the large displacement motions of a cable for in-plane and out-of-plane motions, particularly for cables with a relatively low tension. The axial, flexural and torsional deformations are taken into account in a mathematical model where the

*Corresponding author. Tel.: +386 1 4771 608; fax: +386 1 2518 567.
E-mail address: miha.boltezar@fs.uni-lj.si (M. Boltežar).

0022-460X/$ - see front matter © 2006 Elsevier Ltd. All rights reserved.
doi:10.1016/j.jsv.2006.08.032

analytical formulation and the numerical iterative difference scheme are presented. The model was verified with an experimental simulation and proved to be reliable.

Another significant aspect of the cable dynamics is the consideration of energy dissipation. The mechanisms that have a significant influence on the energy loss are, for example, air resistance, internal material damping and the friction between interwire motions. Although the damping forces are usually relatively small in comparison to the stiffness and inertia forces, they have a significant influence on the dynamics behavior, especially in the resonant regions. Many damping models were developed over the years [4–8], but none of them can be used to describe the damping characteristics of an arbitrary structure. Viscous- and structural-damping models are probably the most widely used models for the characterization of energy loss in structural dynamics.

This paper is organized as follows. In Section 2 the physical and mathematical models with two possible damping models (viscous and structural) are used to characterize the vibrations of cables. The mathematical model is based on the Euler–Bernoulli theory. In Section 3, the Rayleigh coefficients and the loss factor are identified. The verification of the lateral force transmission over straight and curved cables with kinematic support movement is described in Section 4.

2. Theoretical background

An essential characteristic of the mathematical model we used for the dynamical analysis of straight and curved thin cable strands (later cable) is the absence of an axial load. Analyses [9] have shown that cables can, in many cases, be modeled as beams under an axially acting load. In this paper we will consider the dynamic behavior, first of straight bending cable and second of an arbitrary curved cable, both without an axial pre-load. The Euler–Bernoulli beam theory will be used. The emphasis is placed on linear models of damping, i.e., proportional viscous damping in terms of the Rayleigh coefficients and structural damping in terms of the complex modulus of elasticity. The linearity assumption in the two damping models is mainly because of the low-stress regime, the shorter computation time and, most importantly for our research, the use of a relatively simple mathematical model to calculate the vibration transmissibility over relatively complicated cable structures. The physical model we used is shown in Fig. 1.

Euler–Bernoulli equation is used to model the lateral vibrations of a cable,

$$\frac{\partial^2}{\partial x^2}\bar{E}(\omega)I\frac{\partial^2 w(x,t)}{\partial x^2}+c\frac{\partial w(x,t)}{\partial t}+\rho A\frac{\partial^2 w(x,t)}{\partial t^2}=f(x,t), \tag{1}$$

where $f(x,t)$ is the external force per unit length, ρ is the mass density, A is the area of the cross-section, $w(x,t)$ is the lateral displacement at distance x and at time t, I is the second area moment, c is the viscous-damping coefficient and $\bar{E}(\omega)$ is the frequency-dependent complex modulus of elasticity. For the assumption of a viscoelastic material (structural-damping model) the complex modulus of elasticity is given by Eq. (2) [10],

$$\bar{E}(\omega)=E_d(\omega)+\mathrm{i}E_l(\omega)=E_d(\omega)(1+\mathrm{i}\eta(\omega)), \tag{2}$$

where $E_d(\omega)$ is the dynamic modulus, $E_l(\omega)$ is the loss modulus, $\eta(\omega)$ is the loss factor, and $\mathrm{i}=\sqrt{-1}$.

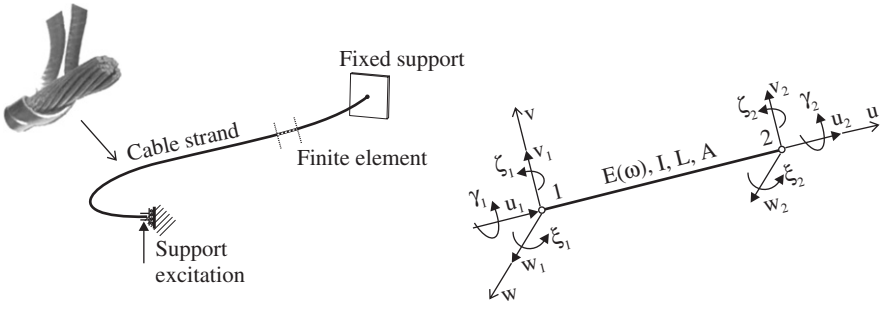

Fig. 1. The physical model for the cable and the finite element.

For modeling the vibrations of the arbitrary curved cable in space, the torsional vibrations are considered with Eq. (3)

$$\frac{\partial}{\partial x}\left(\bar{G}(\omega)J\frac{\partial\theta(x,t)}{\partial x}\right)-c_t\frac{\partial\theta(x,t)}{\partial t}+m_T(x,t)=I_0\frac{\partial^2\theta(x,t)}{\partial t^2}, \tag{3}$$

where $\bar{G}$ is the complex shear modulus, J is the second area polar moment of the cross-section, c_t is the torsional damping coefficient, $\theta(x,t)$ is the angle of twist at a distance x and at time t, I_0 is the moment of inertia per unit length and m_T is the applied twisting moment per unit length. The longitudinal vibrations of the cable can be modeled with

$$\frac{\partial}{\partial x}\left(\bar{E}(\omega)A\frac{\partial u(x,t)}{\partial x}\right)-c_l\frac{\partial u(x,t)}{\partial t}+f_l(x,t)=\rho A\frac{\partial^2 u(x,t)}{\partial t^2}, \tag{4}$$

where $u(x,t)$ is the longitudinal displacement at a distance x and at time t, c_l is the longitudinal damping coefficient and $f_l(x,t)$ is the longitudinal external force. In Eqs. (1), (3) and (4) both damping models can be considered. For the viscously damped model we assume that the damping coefficient $c\neq 0$ and that the loss modulus is equal to zero ($E_l(\omega)=0$). For the assumption of the structural-damping model the conditions are $c=0$ and $E_d(\omega), E_l(\omega)\neq 0$.

For the numerical computation of the vibration transmissibility, the finite elements were used. In the finite-element formulation the following assumptions were made: geometrical linearity, the level of excitation is low, the plane section remains planar after deformations, the material of the cable is homogeneous and isotropic, the displacements and rotations are uncoupled.

Bearing in mind Eqs. (1), (3) and (4), the displacement function $\hat{\mathbf{\Phi}}$ on the finite element can be found with

$$\hat{\mathbf{\Phi}}=\mathbf{N}\mathbf{\Phi}, \tag{5}$$

where $\mathbf{N}$ represents the interpolation functions of the finite element and $\mathbf{\Phi}$ is the nodal displacement. In the case of lateral vibrations of the cable, the third-order Hermitian polynomials are used, and for the torsional and longitudinal vibrations the second-order polynomials are used. According to Fig. 1 the nodal displacements are

$$\mathbf{\Phi}=\{u_1 \quad v_1 \quad w_1 \quad \gamma_1 \quad \zeta_1 \quad \xi_1 \quad u_2 \quad v_2 \quad w_2 \quad \gamma_2 \quad \zeta_2 \quad \xi_2\}^{\mathrm{T}}. \tag{6}$$

The stiffness matrix $\mathbf{k}_i$ and the mass matrix $\mathbf{m}_i$ of the finite element are then derived according to Eqs. (7) and (8), respectively, where index i denotes the ith finite element.

$$\mathbf{k}_i=\mathbf{B}^{\mathrm{T}}\mathbf{D}\mathbf{B}\,\mathrm{d}V, \quad i=1\ldots N, \tag{7}$$

$$\mathbf{m}_i=\mathbf{N}^{\mathrm{T}}\rho\mathbf{N}\,\mathrm{d}V, \quad i=1\ldots N, \tag{8}$$

where $\mathbf{B}$ is the strain–displacement matrix, $\mathbf{D}$ is the stress–strain matrix of the material of volume $\mathrm{d}V$, and N is the number of all the finite elements used along the cable length.

Because of the arbitrary position of the cable in space, the local stiffness and mass matrices of the finite elements must be transformed according to the global coordinate system. For each finite element the transformation can be made within two basic steps, Fig. 2(b) and (c), that formulate the transformation matrix $\mathbf{T}$

$$\mathbf{T}=\begin{bmatrix}\boldsymbol{\lambda} & 0 & 0 & 0\\ 0 & \boldsymbol{\lambda} & 0 & 0\\ 0 & 0 & \boldsymbol{\lambda} & 0\\ 0 & 0 & 0 & \boldsymbol{\lambda}\end{bmatrix}, \tag{9}$$

where $\boldsymbol{\lambda}$ represents the direction-cosine-matrix (rotational matrix). The first step (transformation) can be made with a rotation of the finite element about angle τ around the y axis, where the w-axis is placed on the XZ plane of the global coordinate system. The second transformation can be made around the newly formulated z_τ axis for angle γ. With these two transformations made, the direction-cosine-matrix

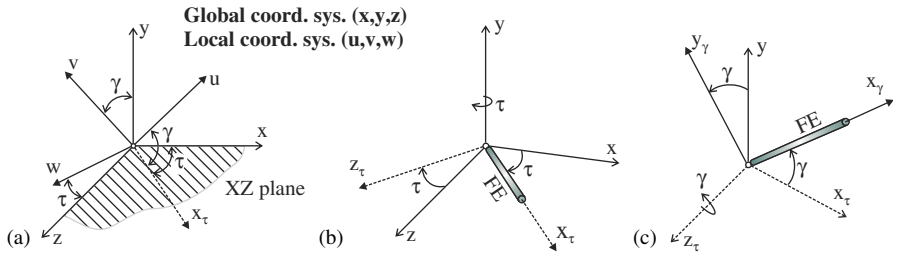

Fig. 2. Transformation from the local coordinate system of the finite element to the global coordinate system of the cable strand: (a) definition of the local and global coordinate systems, (b) positions of the cable after first rotation, (c) positions of the cable after second rotation.

can be defined with Eq. (10).

$$\boldsymbol{\lambda} = \begin{bmatrix} \cos(u,X) & \cos(v,X) & \cos(w,X) \\ \cos(u,Y) & \cos(v,Y) & \cos(w,Y) \\ \cos(u,Z) & \cos(v,Z) & \cos(w,Z) \end{bmatrix} = \begin{bmatrix} \cos(\tau)\cos(\gamma) & \sin(\gamma) & \sin(\tau)\cos(\gamma) \\ -\cos(\tau)\sin(\gamma) & \cos(\gamma) & -\sin(\tau)\sin(\gamma) \\ -\sin(\tau) & 0 & \cos(\tau) \end{bmatrix}. \tag{10}$$

The new, transformed stiffness and mass matrices of the ith element can then be formulated as

$$\mathbf{K}_i = \mathbf{T}_i^{\mathrm{T}} \mathbf{k}_i \mathbf{T}_i,$$

$$\mathbf{M}_i = \mathbf{T}_i^{\mathrm{T}} \mathbf{m}_i \mathbf{T}_i. \tag{11}$$

Bearing in mind the two different damping models and with an assumption of harmonic excitation, Eq. (12) for the viscous-damping model and Eq. (13) for the structural-damping model, can be defined

$$\mathbf{M}\ddot{\mathbf{q}}_v(t) + \mathbf{C}\dot{\mathbf{q}}_v(t) + \mathbf{K}\mathbf{q}_v(t) = \mathbf{F}_v \mathrm{e}^{\mathrm{i}\omega t}, \tag{12}$$

$$\mathbf{M}\ddot{\mathbf{q}}_s(t) + (1+\mathrm{i}\eta)\mathbf{K}\mathbf{q}_s(t) = \mathbf{F}_s \mathrm{e}^{\mathrm{i}\omega t}, \tag{13}$$

where $\mathbf{M}$, $\mathbf{K}$ and $\mathbf{C}$ are the mass, stiffness and viscous-damping matrices of the system of finite elements and $\mathbf{F}$ is the vector of the nodal forces of the finite elements. Index v denotes the mathematical model with the viscous-damping model and s with the structural-damping model. In our study the main point of interest was the amplitude of the response signal in the frequency domain. The particular solution for Eqs. (12) and (13) can be written in the form

$$\mathbf{q}(t) = \mathbf{X}\mathrm{e}^{\mathrm{i}(\omega t+\varphi)}, \tag{14}$$

where $\mathbf{X}$ is the vector of displacement and rotation amplitudes, ω is the excitation frequency and φ is the phase shift. The partially uncoupled equations with partitioning to the known and unknown node displacements and rotations are shown in Eqs. (15) and (16) for the case of the viscous and structural-damping models, respectively.

$$\left(-\omega^2 \begin{bmatrix} \mathbf{M}_{vv} & \mathbf{M}_{vp} \\ \mathbf{M}_{pv} & \mathbf{M}_{pp} \end{bmatrix} + \mathrm{i}\omega \begin{bmatrix} \mathbf{C}_{vv} & \mathbf{C}_{vp} \\ \mathbf{C}_{pv} & \mathbf{C}_{pp} \end{bmatrix} + \begin{bmatrix} \mathbf{K}_{vv} & \mathbf{K}_{vp} \\ \mathbf{K}_{pv} & \mathbf{K}_{pp} \end{bmatrix}\right) \begin{pmatrix} \mathbf{X}_v \\ \mathbf{X}_p \end{pmatrix} = \begin{pmatrix} \mathbf{F}_v \\ \mathbf{F}_p \end{pmatrix}, \tag{15}$$

$$\left(-\omega^2 \begin{bmatrix} \mathbf{M}_{ss} & \mathbf{M}_{sp} \\ \mathbf{M}_{ps} & \mathbf{M}_{pp} \end{bmatrix} + (1+\mathrm{i}\eta) \begin{bmatrix} \mathbf{K}_{ss} & \mathbf{K}_{sp} \\ \mathbf{K}_{ps} & \mathbf{K}_{pp} \end{bmatrix}\right) \begin{pmatrix} \mathbf{X}_s \\ \mathbf{X}_p \end{pmatrix} = \begin{pmatrix} \mathbf{F}_s \\ \mathbf{F}_p \end{pmatrix}. \tag{16}$$

The indices v and s denotes the unknown node variables for the considered viscous and structural-damping models, respectively, and index p is used to denote the supported node variables. The main interest is the unknown value of the force amplitude $\mathbf{F}_p$ at the fixed support while the kinematic excitation $\mathbf{X}_p$ is applied at the other fixed support, Fig. 1.

By setting the external forces $\mathbf{F}_v$ and $\mathbf{F}_s$ to zero, and with the known kinematic excitation $\mathbf{X}_p \neq \mathbf{0}$, we can derive the expression for the force amplitude in fixed supports for:

1. the viscous-damping model:

$$\mathbf{X}_v = (\mathbf{K}_{vv} + \mathrm{i}\omega\mathbf{C}_{vv} - \omega^2\mathbf{M}_{vv})^{-1}\,(\omega^2\mathbf{M}_{vp}\mathbf{X}_p - \mathbf{K}_{vp}\mathbf{X}_p - \mathrm{i}\omega\mathbf{C}_{vp}\mathbf{X}_p), \tag{17}$$

$$\mathbf{F}_p = -\omega^2(\mathbf{M}_{pv}\mathbf{X}_v + \mathbf{M}_{pp}\mathbf{X}_p) + \mathrm{i}\omega(\mathbf{C}_{pv}\mathbf{X}_v + \mathbf{C}_{pp}\mathbf{X}_p) + \mathbf{K}_{pv}\mathbf{X}_v + \mathbf{K}_{pp}\mathbf{X}_p. \tag{18}$$

2. the structural-damping model:

$$\mathbf{X}_s = ((1 + \mathrm{i}\eta)\mathbf{K}_{ss} - \omega^2\mathbf{M}_{ss})^{-1}\,(\omega^2\mathbf{M}_{sp}\mathbf{X}_p - (1 + \mathrm{i}\eta)\mathbf{K}_{sp}\mathbf{X}_p), \tag{19}$$

$$\mathbf{F}_p = -\omega^2(\mathbf{M}_{ps}\mathbf{X}_s + \mathbf{M}_{pp}\mathbf{X}_p) + (1 + \mathrm{i}\eta)(\mathbf{K}_{ps}\mathbf{X}_s + \mathbf{K}_{pp}\mathbf{X}_p). \tag{20}$$

For the computation of the vibration transmissibility the transfer response function in terms of the apparent mass (TRFAM, [11]) was computed and measured according to Eqs. (18) and (20). For the discrete frequency ω_i the TRFAM can be computed as

$$\mathrm{TRFAM}(\omega_i) = \frac{F_{p(i)}}{X_{p(i)}}, \tag{21}$$

where $F_{p(i)}$ and $X_{p(i)}$ represent the force and the displacement amplitude at the discrete frequency ω_i.

3. Identification of the damping parameters

For the two damping models used, the damping matrix $\mathbf{C}$ in Eq. (12), and the loss factor η in Eq. (13) have to be identified.

3.1. Identification of the damping matrix

The viscous damping is modeled in the form of proportional (equivalent) Rayleigh damping, where the Rayleigh coefficients α and β have to be identified.

$$\mathbf{C} = \alpha\mathbf{M} + \beta\mathbf{K}. \tag{22}$$

It can be shown from the orthogonality principle [12] that the relation between the ith damping ratio ζ_i and the ith natural frequency ω_i can be written in the form

$$\zeta_i = \frac{\alpha}{2\omega_i} + \frac{\beta\omega_i}{2}. \tag{23}$$

With two estimated natural frequencies and damping ratios from the measured signal, the Rayleigh coefficients α and β can be estimated. In our study, the modal parameters were identified with the least-squares time-domain method process [13,14] of the measured impulse response in the time domain at the clamped support of the cable. The response of an m-degree-of-freedom transient is considered to be in the form

$$y(t) = A_0 + \sum_{k=1}^{m} A_k \mathrm{e}^{-\alpha_k t}\sin(\omega_k t + \phi_k), \quad k = 1, 2, \ldots, m, \tag{24}$$

where A_0 is the zero-offset correction, A_k is the participation factor of the kth mode, α_k is the damping of the kth mode and ω_k and ϕ_k are the frequency and phase angle of the kth mode.

After identification of the modal parameters, the values of the Rayleigh coefficients α and β were obtained with the least-squares fitting process of the modal parameters. For this purpose the pseudo-inverse routine was

used, see Eqs. (25)–(27), where the notation $\sim$ represents the estimated values from the measurements.

$$\begin{bmatrix} \tilde{\zeta}_1 \\ \tilde{\zeta}_2 \\ \vdots \\ \tilde{\zeta}_m \end{bmatrix} = \begin{bmatrix} \dfrac{1}{2\tilde{\omega}_1} & \dfrac{\tilde{\omega}_1}{2} \\ \dfrac{1}{2\tilde{\omega}_2} & \dfrac{\tilde{\omega}_2}{2} \\ \vdots & \vdots \\ \dfrac{1}{2\tilde{\omega}_m} & \dfrac{\tilde{\omega}_n}{2} \end{bmatrix} \begin{bmatrix} \alpha \\ \beta \end{bmatrix}, \tag{25}$$

and with simplified matrix notation

$$\mathscr{Z} = \mathscr{A}\mathscr{C}. \tag{26}$$

The pseudo-inverse process gives the estimated values of α and β in a vector $\mathscr{C}$

$$\mathscr{C} = (\mathscr{A}^{\mathrm{T}}\mathscr{A})^{-1}\mathscr{A}^{\mathrm{T}}\mathscr{Z} = \mathscr{A}^{+}\mathscr{Z}. \tag{27}$$

The graphical representation for the theoretical values of the damping ratios versus the natural frequencies for the proportional Rayleigh damping model is shown in Fig. 3. The graph clearly shows the influence of the mass matrix (coefficient α) and the stiffness matrix (coefficient β) on the dissipation of energy from the model. The curve that represents the influence of both the mass and the stiffness matrix is the most important because the coefficients α and β were chosen to best fit the measured damping ratios. In the large majority of cases the proportional damping can only be acceptable for the use in narrow frequency range. Our studies showed that when the wider frequency range is considered, better approximation can be made (especially in the lower-frequency region) if the coefficient α is set according to the measured damping ratio of the first measured natural frequency. Afterwards, coefficient β is determined with the least-square process, see Eqs. (25)–(27), considering the damping ratios of the second natural frequency to the highest accounted natural frequency in the measurements. The process described was used for all the identifications of the coefficients α and β.

3.2. Identification of the loss factor

Many different methods have been developed to identify the complex modulus and the loss factor. The standing-wave method and the non-resonant method are often used to identify the complex modulus. Oyadiji and Tomlinson [15] reported the identification of the loss factor with the results from the resonant and non-resonant methods with an absolute error between 0.4% and 8%. The only restriction is that the value of the loss factor is less than 0.4. In our study the loss factor was estimated from the Nyquist plot of the measured TRFAM. For linear systems, the Nyquist plot (for cases of receptance, mobility and accelerance) should in the

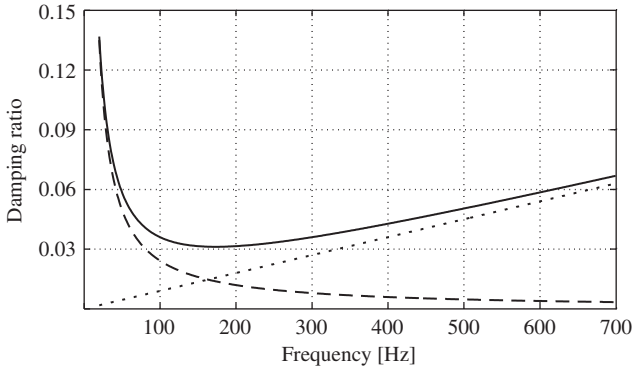

Fig. 3. Influence of the mass and stiffness matrix on the damping ratio for the proportional Rayleigh damping model: mass-proportional damping (−−), stiffness-proportional damping (···), both mass-proportional and stiffness-proportional damping (—).

resonant region take the approximate shape of a circle [16]. From the theoretical point, any possible deviation from a circle, for example, an ellipse, can be caused by structural nonlinearities in the stiffness or damping terms, which we did not observe.

Our studies showed that for linear case the TRFAMs in Nyquist plot (resonant regions) approximate to a shape of a circle, where the deviation from the measured Nyquist circle can be approximated by an analytical circular function. The process is schematically presented in Fig. 4. The main idea is to estimate the natural frequency ω_0 and the boundary frequencies ω_1 and ω_2 from the fitted circular function for each resonant region. The loss factors at the natural frequencies can be estimated with Eq. (28)

$$\eta_{(k)} = \frac{\omega_{2(k)}^2 - \omega_{1(k)}^2}{2\omega_{0(k)}^2}, \tag{28}$$

where the index k is the kth resonant region (natural frequency). Henwood [17] has shown that a loss factor of less than 0.4 can be approximated with the known damping ratios of the viscous-damping model by $\eta \approx 2\zeta$. Bearing this relation in mind we can compare the two identification processes, i.e., the least-squares time-domain method process and the identification from a Nyquist plot in the frequency domain. The only restriction with this kind of identification process is that the natural frequencies are not closely spaced.

3.3. Frequency dependence of the dynamic modulus of elasticity

The frequency dependence of the dynamic modulus of elasticity was identified with the adaptive process, Fig. 5. The computed values of the natural frequencies were adapted to the measured ones. The iteration

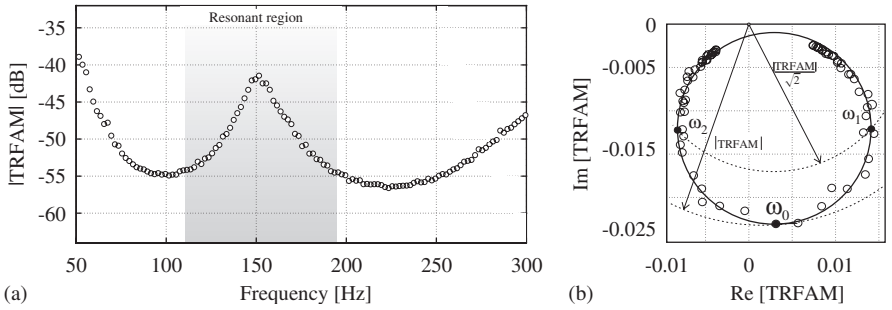

Fig. 4. Representation of the measured TRFAM: (a) Bode diagram of the TRFAM (○), (b) the concept of loss-factor identification from a Nyquist plot, TRFAM (○) and fitted circular function (—). Natural frequency ω_0 and boundary frequencies ω_1, ω_2 are denoted with (•).

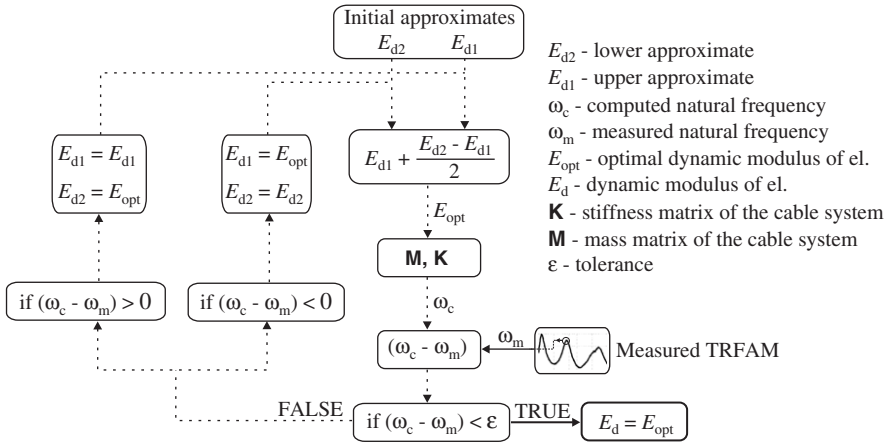

Fig. 5. The adaptive process (- - -) for identification of the frequency dependence of the dynamic modulus of elasticity E_d.

Fig. 6. Both fixed ends for measurement of the vibrations of the cable.

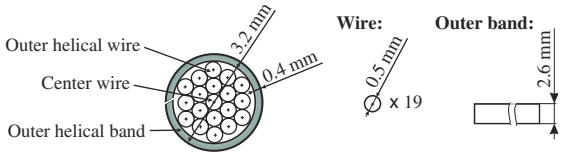

Fig. 7. Cross-section of the cable with the helical wires and the outer band.

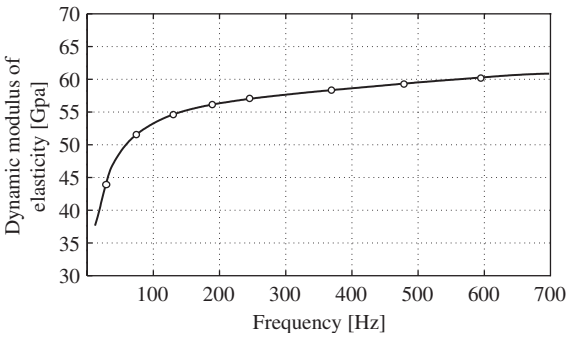

Fig. 8. Interpolation curve for the frequency dependence of the dynamic modulus of elasticity (–), through the measured natural frequency (○).

Table 1
Geometrical characteristics of the cable

I (m^4)	ρ (kg/m^3)	d_{cw} (m)	d_{ow} (m)	D_{ib} (m)	D_{ob} (m)	φ_1 (°)	φ_2 (°)	s
3.1083×10^{-12}	7650	0.0005	0.0005	0.0024	0.0032	85	60	19

process continued until the differences between the computed and measured values of the natural frequencies were half of the frequency resolution in the measured TRFAM, which was 0.25 Hz.

4. Experimental case study

The suitability of the mathematical model used for the straight and curved cables with no axial pre-load was tested with an experiment. Both fixed ends of the physical model are shown in Fig. 6. The boundary conditions

Table 2
Difference of the damping ratios for the two identification methods, for length $l = 0.253\,\mathrm{m}$

Mode number	1	2	3
LSM_t	0.0323	0.0106	0.0103
NY_f	0.029	0.0135	0.012

Table 3
Difference of the damping ratios for the two identification methods, for length $l = 0.328\,\mathrm{m}$

Mode number	1	2	3	4
LSM_t	0.024	0.00984	0.0097	0.0098
NY_f	0.021	0.011	0.014	0.012

Table 4
Difference of the damping ratios for the two identification methods, for length $l = 0.4\,\mathrm{m}$

Mode number	1	2	3	4	5
LSM_t	0.071	0.028	0.0342	0.0315	0.027
NY_f	0.062	0.039	0.035	0.0318	0.034

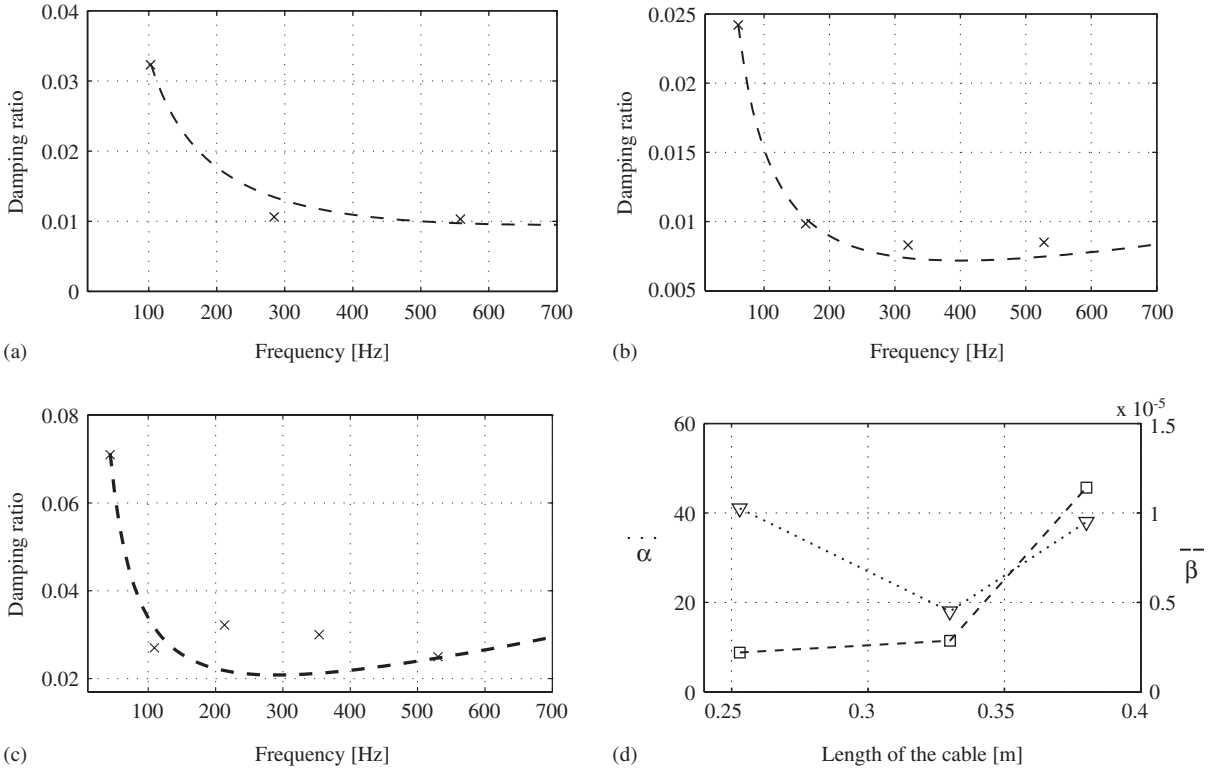

Fig. 9. Approximated Rayleigh function (– – –) for measured damping ratios at natural frequencies (○) for straight cable lengths: (a) 0.253 m, (b) 0.328 m and (c) 0.4 m; (d) changes of Rayleigh coefficients $\alpha(\cdots)$ and $\beta(- - -)$ with different lengths of cables.

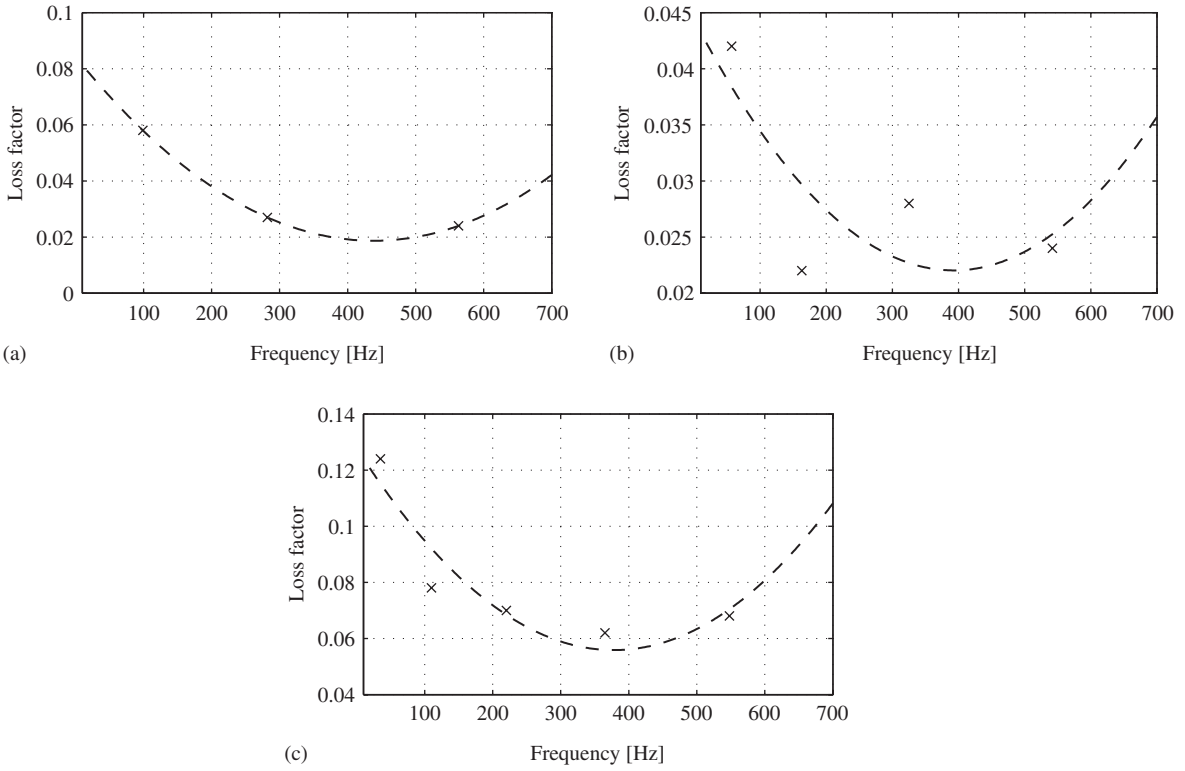

Fig. 10. Approximation of loss factor for straight cable with quadratic function. Length of cable: (a) 0.253 m, (b) 0.328 m and (c) 0.4 m.

were the same for the straight and curved cables. The support excitation is obtained with the controlled electrodynamic shaker and the force amplitude is measured at the fixed support with a dynamometer. The cross-section of the cable is shown in Fig. 7.

The verification of the mathematical model was made on straight cables with three different lengths and on an initially curved cable. Two cases of curved cable were studied, i.e., the cable in one plane and the cable in space. The different lengths of the straight cable were analyzed for the purpose of defining the dependence of the Rayleigh coefficient on the length of the cable. The cable was excited with a broadband noise signal in the frequency range from 10 to 700 Hz, with the RMS value of the excitation signal equal to $5\,\mathrm{m\,s^{-2}}$.

4.1. Straight cable

The lengths of the analyzed straight cables were 0.253, 0.328 and 0.4 m. The identification curve of the frequency dependence of the dynamic modulus of elasticity (the adaptive process is shown in Fig. 5) was proved to be valid for all the cases of analyzed cable shapes, and is shown in Fig. 8.

The second area moment can be calculated from the known geometrical characteristics of the cable, including the helical angle of the outer wires and the outer band, with Eq. (29).

$$I = I_c + I_b = \frac{\pi}{64}(s\,d_{\mathrm{ow}}^4 \sin\varphi_1^4 + d_{\mathrm{cw}}^4) + \frac{\pi}{64}(D_{\mathrm{ob}}^4 - D_{\mathrm{ib}}^4)\sin\,\varphi_2. \tag{29}$$

I_c is the second area moment of the cable wires and I_b is the second area moment of the outer band. d_{cw} is the diameter of the center wire, d_{ow} is the diameter of the outer wires, D_{ib} and D_{ob} are the inner and outer diameter of the band, respectively, s is the number of outer wires and φ_1 and φ_2 are the helical angles of the outer wires and the band according to the center wire of the cable (the cable is straight at $\varphi = 90^\circ$). The mass

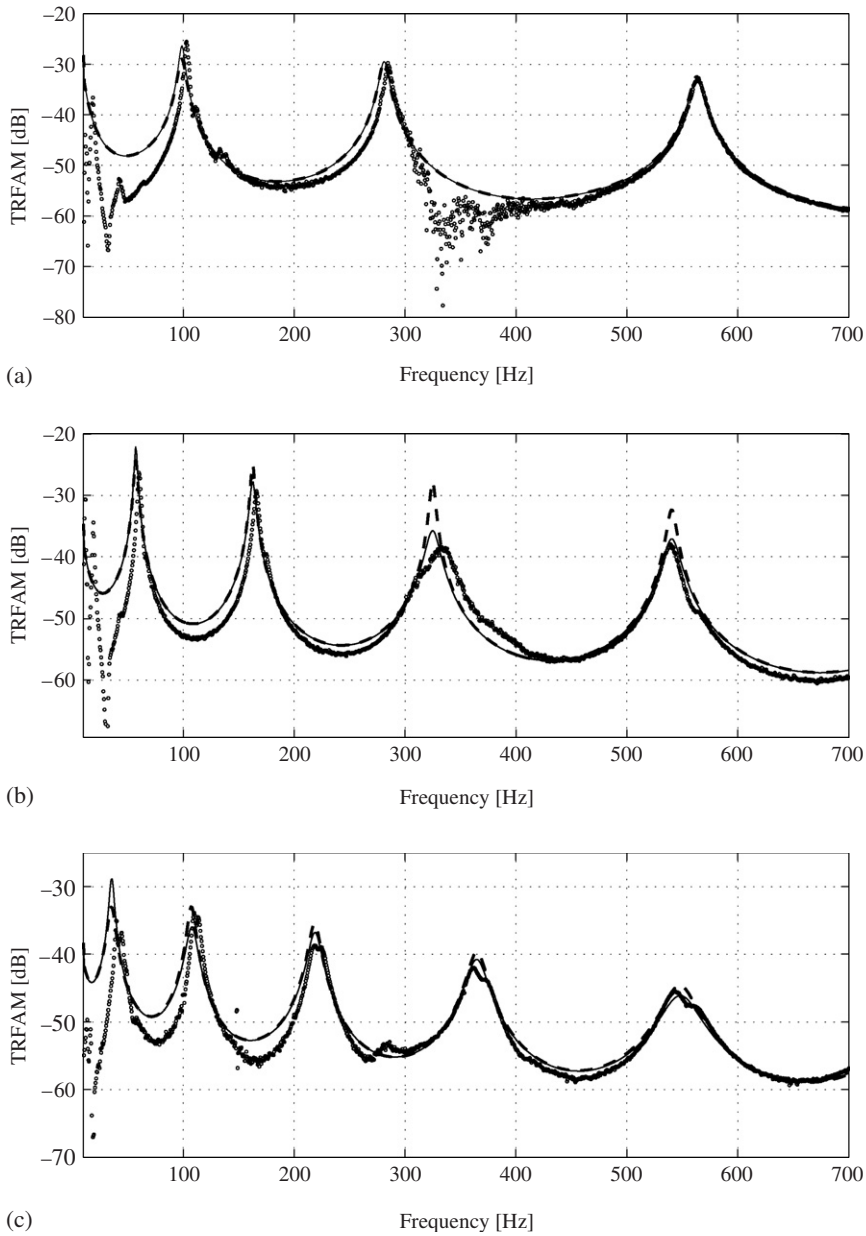

Fig. 11. The TRFAM for the straight cable of length (a) 0.253 m, (b) 0.328 m and (c) 0.4 m: (○) measurement, (—) structural-damping model, (– – –) viscous-damping model.

density of the material used for the studied cable was calculated using the known mass and volume of the cable wires and the outer band. The estimated geometrical values are given in Table 1.

The differences in the identified damping ratios, using the least-squares fitting method (denoted by LSM_t) and the Nyquist plot (denoted by NY_f), are shown in Tables 2–4 for the straight cables of different lengths. The approximation of the Rayleigh coefficients α and β were made using the process described in Section 3.1, and they are shown in Fig. 9(a–c) for the straight cables. The dependence of the Rayleigh coefficients on the lengths of the cables is shown in Fig. 9(d). The identified loss factors and the approximated quadratic function are shown in Fig. 10(a–c). The reason for using the approximated quadratic function is in the fact that the

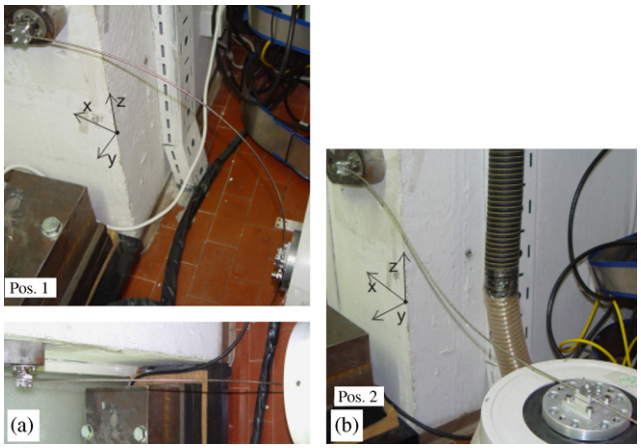

Fig. 12. Geometry of the cable for studying the in-plane vibrations: (a) position one, (b) position two.

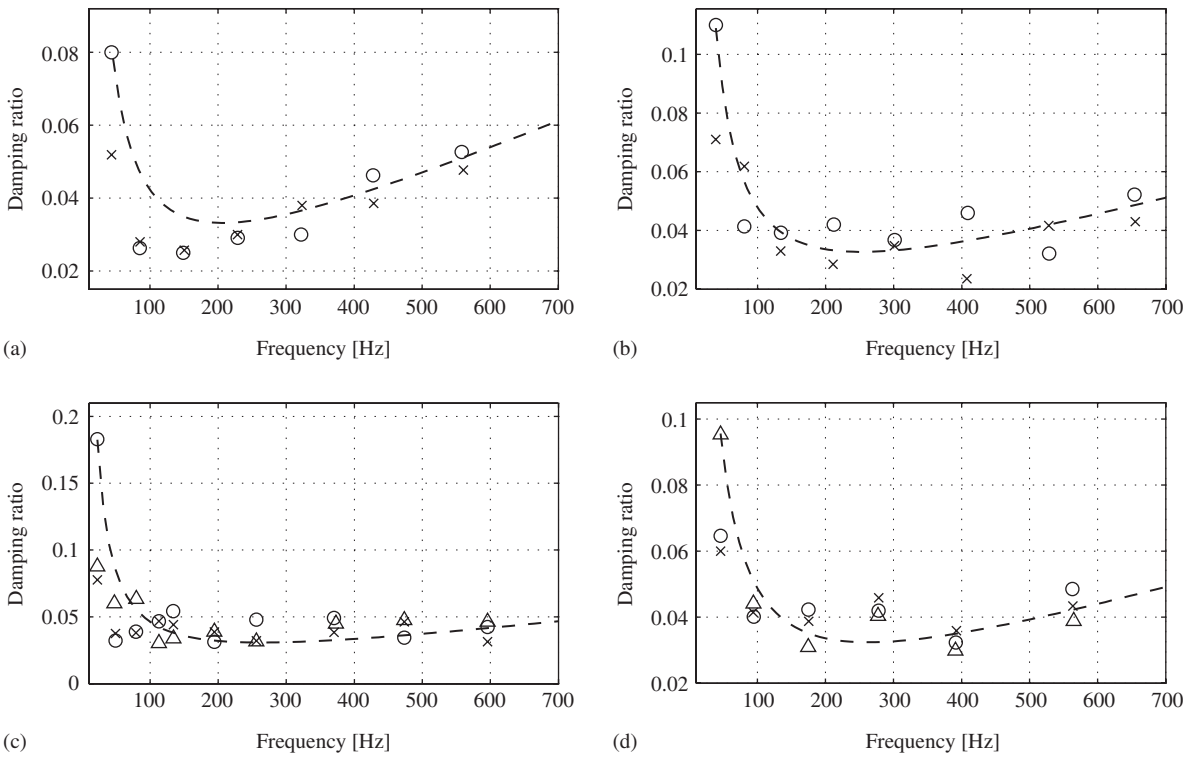

Fig. 13. Approximation of damping ratios for direction $x(\circ)$, $y(\triangle)$ and $z(\times)$ with Rayleigh damping model. Position of cable: (a) first, (b) second, (c) third and (d) fourth.

maxima of $\eta(\omega)$ is at the inflexion point of the $E_d(\omega)$ function [10]. The shape of the identified curve for $E_d(\omega)$ "insinuate", Fig. 8, that the quadratic-shape function can be used for the approximation of the $\eta(\omega)$ in the least-squares fitting process.

The experimental verification of the mathematical model for the lateral vibrations of the straight cables in terms of the TRFAM, for the z measurement direction, is shown in Fig. 11(a–c), where the differences between the measured TRFAM and the computed TRFAM, with two different model of damping, can be seen.

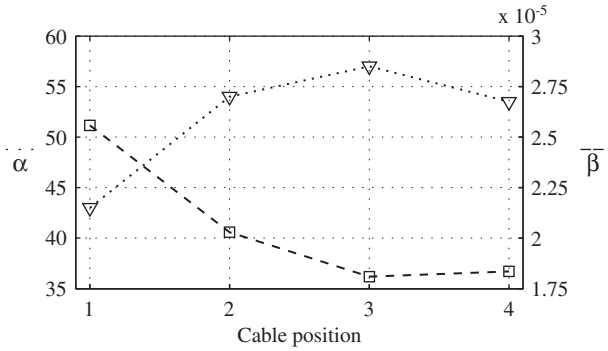

Fig. 14. Values for Rayleigh coefficients $\alpha(\cdots)$ and $\beta(- - -)$ for different positions of cable.

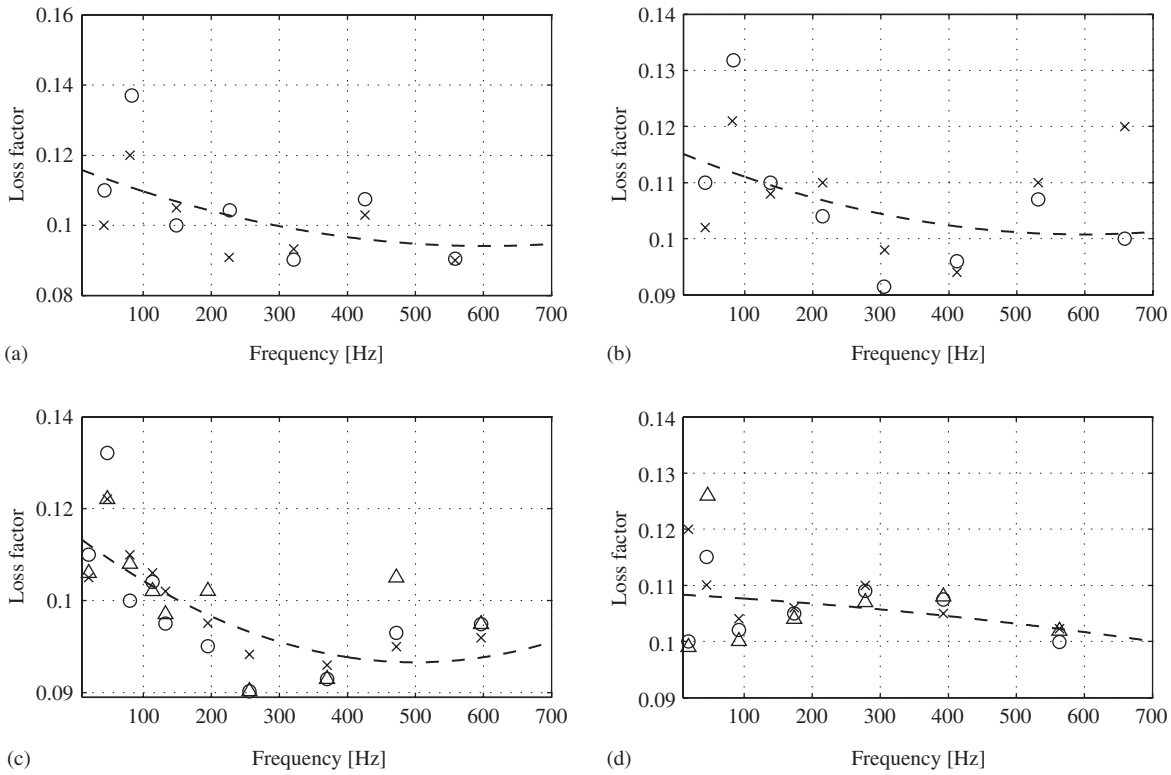

Fig. 15. Approximation of loss factor for direction $x(\circ)$, $y(\triangle)$ and $z(\times)$ with quadratic function. Position of cable: (a) first, (b) second, (c) third and (d) fourth.

4.2. Curved cable

The mathematical model used for the cable with no axial pre-load was also verified for an arbitrary curved cable. Two different shape settings of the curved cable were studied: (i) in-plane and (ii) out-of-plane vibrations. The shapes of the studied cables were transmitted to the mathematical model with the help of the measuring arm. The points were taken along the cable at intervals of 1 cm. This measuring procedure was repeated three times, and the final shape of the curved cable used in the mathematical model was obtained with an approximation using the measured points. The differences between the shape considered in the

mathematical model and the shape of the experimental setting is estimated to have an absolute value of 0.8 mm in the direction perpendicular to the axis of the cable.

4.2.1. In-plane vibrations

Two different shapes of curved cable were analyzed for in-plane vibrations. The shapes (positions) are shown in Fig. 12(a,b). The length of the cable in the first position was 0.63 m, and in the second position it was 0.64 m. The values of the approximated Rayleigh function (Eq. (23)) are shown in Fig. 13(a,b) for the first and second positions of the cable. The approximated curve is based on the values of both measured directions, y and z. This gives us independent values of the coefficients α and β with regard to the computed directions x and z.

The values of the estimated Rayleigh coefficients, which were later used in the TRFAM analysis, are shown in Fig. 14 for positions one and two.

The frequency dependence of the loss factor was identified from the Nyquist plot for each natural frequency, see Section 3.2. The approximated curves of the loss factors for the first and second positions of the cable are shown in Fig. 15(a,b). The approximations were made with regards to both measured directions and were used in the subsequent TRFAM analysis.

The experimental verification of the vibration transmissibility in terms of the TRFAM measurement is shown in Figs. 16 and 17 for the analyzed in-plane positions of the cable.

4.2.2. Out-of-plane vibrations

The out-of-plane motions were studied at two different positions of the cable, shown in Figs. 18 and 19. The length of the cable in the third position was 0.68 m, and in fourth position it was 0.55 m. The Rayleigh

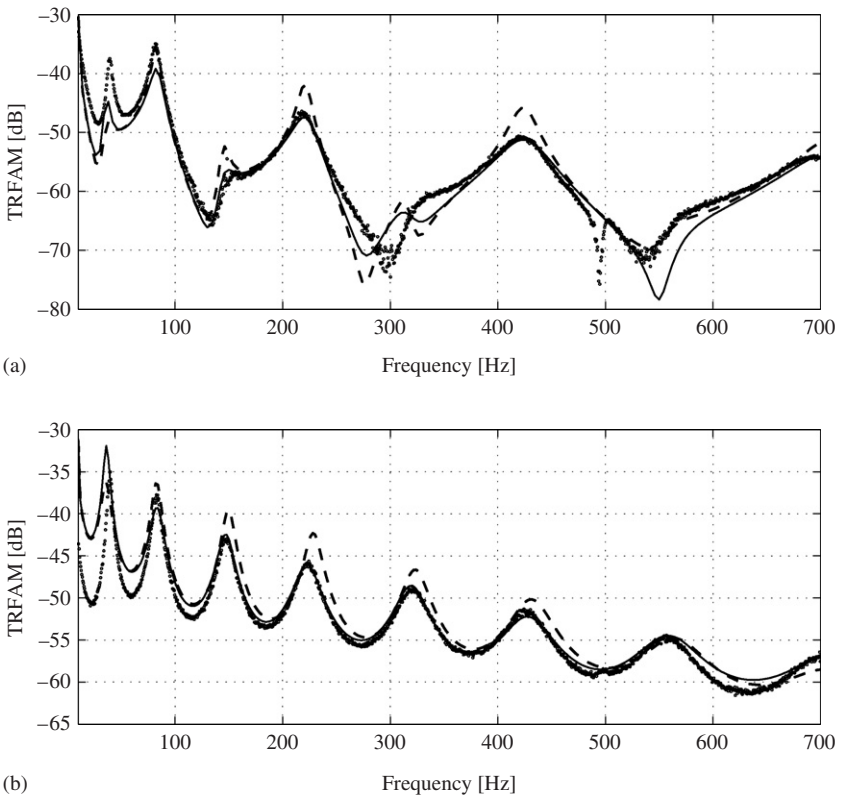

Fig. 16. The TRFAM for the first position of cable: (○) measurement, (—) structural-damping model, (– – –) viscous-damping model. Directions of force measurement: (a) **x**, (b) **z**.

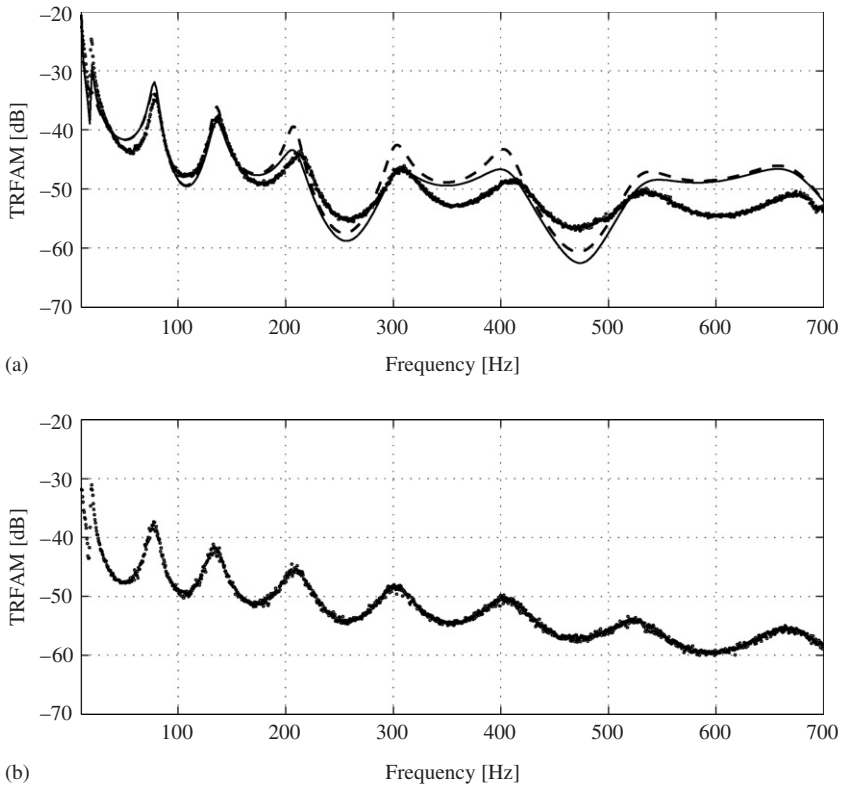

Fig. 17. The TRFAM for the second position of cable: (○) measurement, (—) structural-damping model, (– – –) viscous-damping model. Directions of force measurement: (a) **x**, (b) **z**.

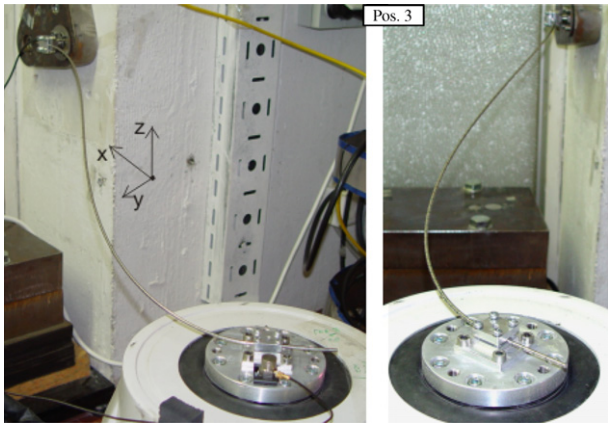

Fig. 18. Geometry of the cable for studying out-of-plane vibrations, position three.

coefficients were identified with the same procedure used for the straight and in-plane curved cable, see Sections 4.1 and 4.2.1. The results of the approximations are shown in Fig. 13(c,d). The values of the estimated Rayleigh coefficients for positions three and four are shown in Fig. 14(cable position 3, 4). The identification of the frequency dependence of the loss factor is shown in Fig. 15(c,d).

The experimental verification for the mathematical model with both presented damping models is shown in Figs. 20 and 21 for all the measured direction.

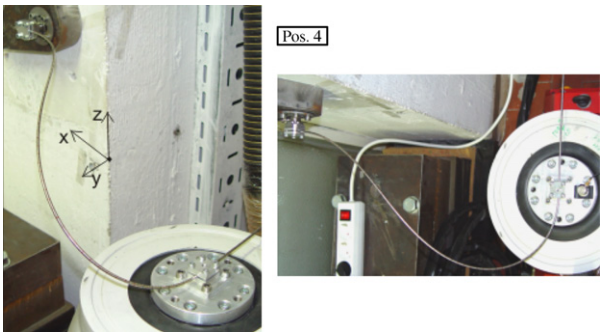

Fig. 19. Geometry of the cable for studying out-of-plane vibrations, position four.

5. Conclusions

This paper presents an analysis of the lateral vibrations of straight and curved cables with no axial pre-load. The excitation in terms of support motions was in the direction perpendicular to the axis of the cable. The dissipation of the energy was approximated with two different models of damping, i.e., the viscous Rayleigh model and the structural-damping model. Three different lengths of cable were analyzed for the purpose of studying the influence of cable length on the identified Rayleigh coefficients. The results in Fig. 9(d) for the straight cables and in Fig. 14 for the curved cables show that the changes in the Rayleigh coefficients α and β, due to the different lengths, are not negligible and must be considered in the mathematical model. In order to identify the damping ratios, the least-squares fitting method was used. The loss factors were identified from the Nyquist plot, where the measured TRFAMs were approximated with a circular function. The frequency-dependent curve of the loss factor was obtained from an approximation using a quadratic polynomial. The main reason for choosing the quadratic polynomial was the shape of the identification curve of the dynamic modulus of elasticity. From theory [10], the maximum of the loss-factor curve should be at the inflexion point of the frequency-dependence curve of the modulus of elasticity. We estimated that there was one inflexion point at approximately 15 Hz. It can be seen from Fig. 10(a–c), for the straight cables, and from Fig. 13(a–d), for the curved cables, that real systems do not always show the same behavior in terms of the point of the maximum of the loss-factor curve approximation, because no distinct maximum value can be seen from the figures at the inflection point of the modulus of elasticity. The frequency dependence of the dynamic modulus of elasticity was estimated by an adaptive process and was proven to be the same for all the shapes and lengths of the cables studied.

The measurement of the TRFAM showed that the viscous-damping model proved to increase in the resonant regions in comparison to the structural-damping model. It is also clear that the difference between the measured and the computed TRFAM is smaller if the coefficient α is estimated by the process described in Section 3.1.

The mathematical model used was shown to be reliable for an estimation of the natural frequency of the cables. The model was verified with TRFAM measurements for straight and curved cables with in-plane and out-of-plane vibrations. Figs. 16, 17, 20 and 21 show the differences between the measured and computed TRFAMs (curved cable) with both damping models. The main factors that could have a significant influence on the inequality of the TRFAMs can be listed in three categories. The first influence could be the inexact transmission of the cable geometry from the experiment to the geometry used in the mathematical model. The second influence could be the inexact approximation of the boundary conditions accounted in the mathematical model, compared to the experimental setup. In particular for our case, where the kinematic excitation of the cable support was introduced, the rotational degree of freedom could arise at the point of the fixed support (the point of kinematic excitation). This causes the boundary conditions, considered in the experimental measurement, to have a lower local "boundary" stiffness than those accounted in the mathematical procedure. We suspect that this is the main reason for the error that is introduced in the lower-frequency regions, starting from theory [16]. In addition, the dynamical models are in general stiffness-controlled in the lower-frequency regions, which also correspond to the influence of the boundary

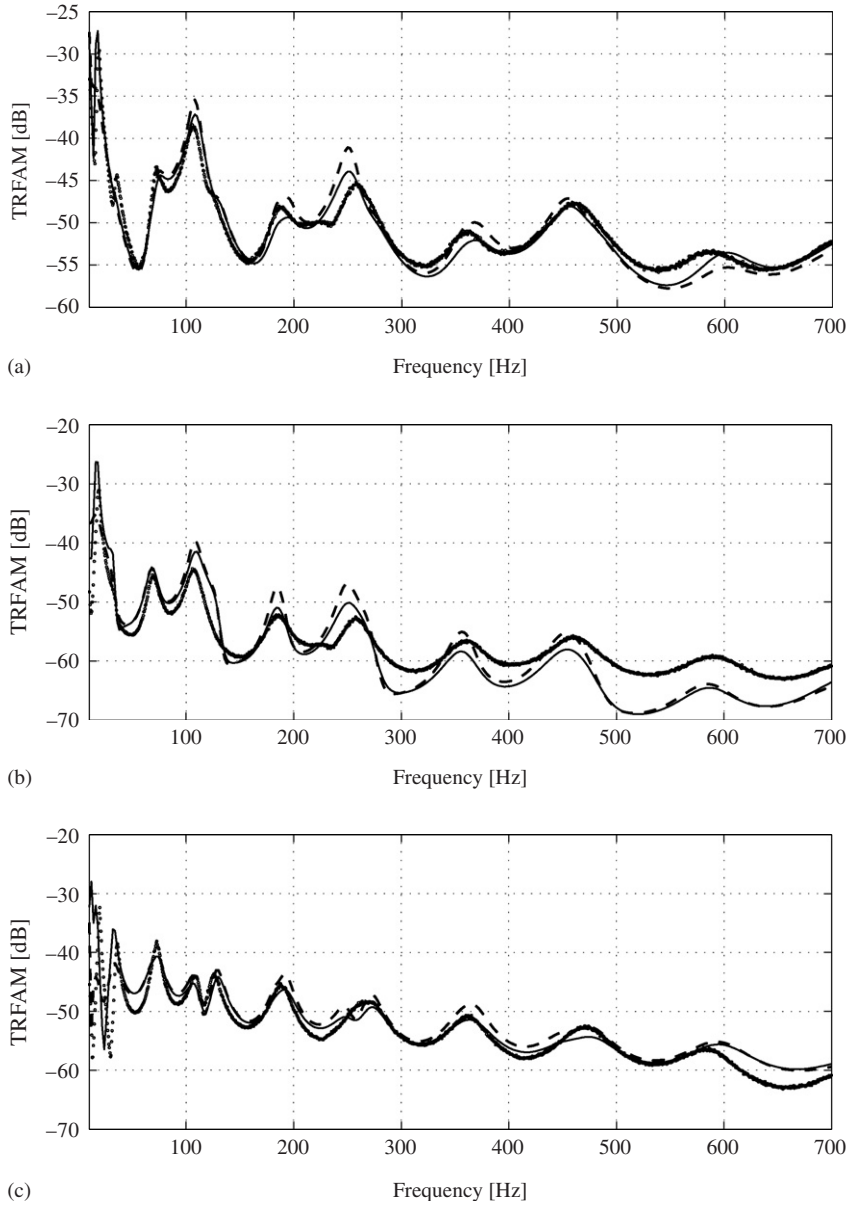

Fig. 20. The TRFAM for the third position of cable: (○) measurement, (—) structural-damping model, (– – –) viscous-damping model. Directions of force measurement: (a) **x**, (b) **y** and (c) **z**.

conditions. The third influence of the error could arise directly from the used mathematical model. The mathematical model is relatively simple and is here used to analyze the transmissibility over very complex cable structures.

Overall, the mathematical model with the structural-damping model is suitable for estimating the TRFAM with an error in the amplitude of the TRFAM (linear) from 0% to approximately ±30% in some frequency regions. The biggest difference between the measured and computed TRFAM is for the second position of the cable in the x measurement direction and for fourth position of the cable in the z measurement direction. For the two damping models used, the structural-damping model produced better results in terms of the measurements of the TRFAM. The TRFAMs with the viscous Rayleigh model tend to increase in the resonant regions compared to the measurements for the straight and curved cables.

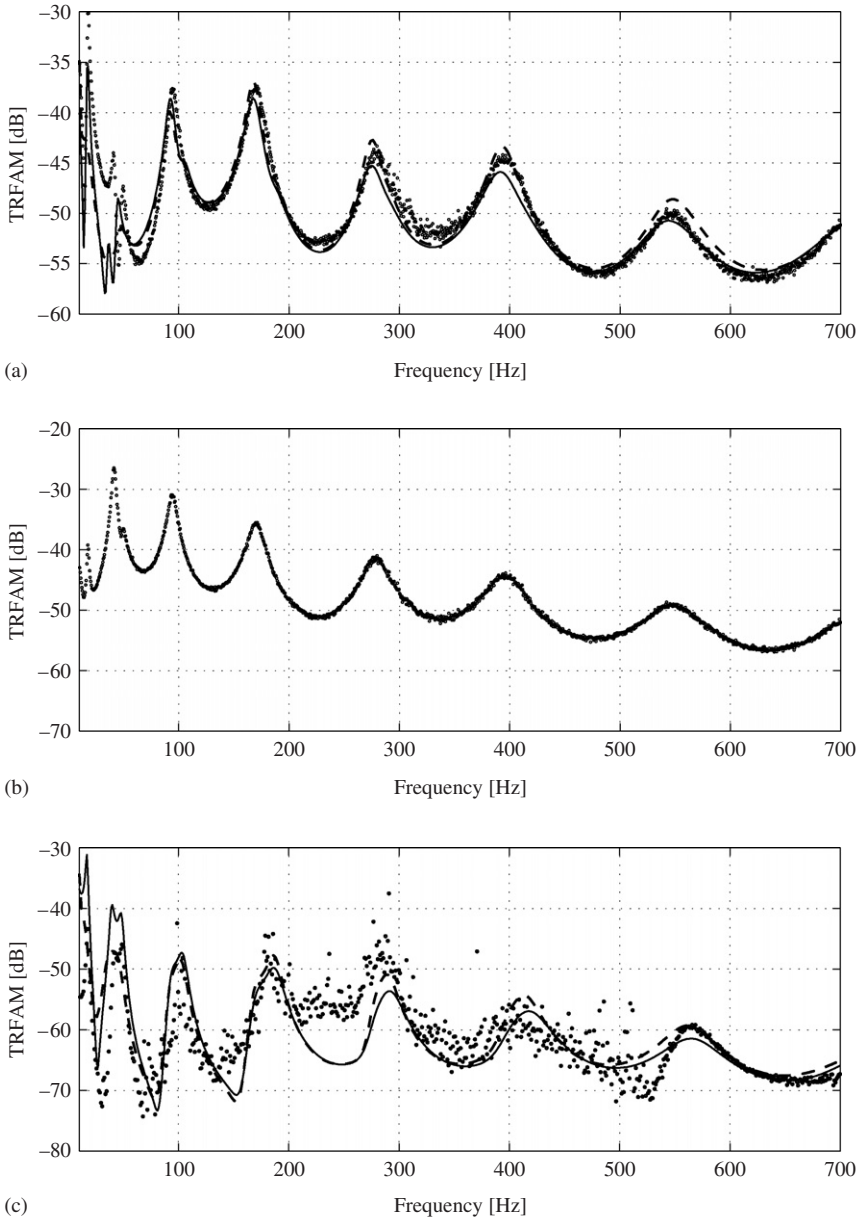

Fig. 21. The TRFAM for the fourth position of cable: (○) measurement, (—) structural-damping model, (– – –) viscous-damping model. Directions of force measurement: (a) **x**, (b) **y** and (c) **z**.

Acknowledgements

The support of Cimos d.d., Ministry of the economy and Ministry of Education and Sport of the Republic of Slovenia is greatly acknowledged.

References

[1] G.A. Costello, *Theory of Wire Rope*, Springer, Berlin, 1990.
[2] A. Nawrocki, M. Labrosse, A finite element model for simple straight wire rope strands, *Computers and Structures* 77 (2000) 345–359.

[3] C.G. Koh, Y. Rong, Dynamic analysis of large displacement cable motion with experimental verification, *Journal of Sound and Vibrations* 272 (2004) 187–206.
[4] J. Woodhouse, Linear damping models for structural vibrations, *Journal of Sound and Vibration* 215 (3) (1998) 547–569.
[5] S. Adhikari, Damping Models for Structural Vibration, PhD thesis, Engineering Department, Cambridge University, 2000.
[6] S. Adhikari, J. Woodhouse, Identification of damping—part 1: viscous damping, *Journal of Sound and Vibration* 243 (1) (2001) 43–61.
[7] C.W. Bert, Material damping: an introductory review of mathematical models, measures and experimental techniques, *Journal of Sound and Vibration* 29 (2) (1973) 129–153.
[8] N.M.M. Maia, J.M.M. Silva, A.M.R. Ribeiro, On a general model for damping, *Journal of Sound and Vibration* 218 (5) (1998) 749–767.
[9] N. Barbieri, O.H. de Souza, R. Barbieri, Dynamical analysis of transmission line cables—part 1: linear theory, *Mechanical Systems and Signal Processing* 18 (2004) 659–669.
[10] T. Pritz, Frequency dependences of complex moduli and complex Poisson's ratio of real solid materials, *Journal of Sound and Vibration* 214 (1) (1998) 83–104.
[11] Personal communication with prof N.M.M. Maia, Department of Mechanical Engineering, Instituto Superior Técnico, Lisboa, Portugal.
[12] I. Chowdhury, S.P. Dasgupta, Computation of Rayleigh damping coefficients for large systems, Department of Civil Engineering, Indian Institute of Technology, India, 1998.
[13] W.R. Smith, Least-squares time-domain method for simultaneous identification of vibration parameters from multiple free-response record, American Institute of Aeronautics and Astronautics, Inc., California, 1981, pp. 194–201.
[14] N. Jakšič, M. Boltežar, An approach to parameter identification for a single-degree-of-freedom dynamical system based on short free acceleration response, *Journal of Sound and Vibration* 250 (3) (2002) 465–483.
[15] S.O. Oyadiji, G.R. Tomlinson, Determination of the complex moduli of viscoelastic structural elements by resonance and non-resonance methods, *Journal of Sound and Vibration* 101 (3) (1985) 277–298.
[16] N.M.M. Maia, J.M.M. e Silva, Theoretical and experimental modal analysis, *Instituto Superior Téhnico*, *Portugal*, Wiley, New York, 1997.
[17] D.J. Henwood, Approximating the hysteretic damping matrix by viscous matrix for modeling in the time domain, *Journal of Sound and Vibration* 254 (3) (2002) 575–593.